SEMARAK ILMU PUBLISHING

CFD Letters

Journal homepage:
https://semarakilmu.com.my/journals/index.php/CFD_Letters/index
ISSN: 2180-1363

Numerical Analysis and Experimental Validation of Trimaran and Pentamaran Resistance at Various Separation Distances

Egi Yuliora[1], I Ketut Aria Pria Utama[1,*], I Ketut Suastika[1]

[1] Department of Naval Architecture, Faculty of Marine Technology, Institut Teknologi Sepuluh Nopember (ITS), Surabaya 60111, Indonesia

ARTICLE INFO

Article history:
Received 17 January 2024
Received in revised form 15 February 2024
Accepted 10 March 2024
Available online 31 October 2024

Keywords:
CFD; EFD; Multihull; NPL-4b; Resistance

ABSTRACT

Trimaran and pentamaran are multihull types with an odd number of hulls, namely three and five hulls, generally consisting of one center hull and two or four side hulls smaller than the center hull, which can reduce ship resistance. The trimaran and pentamaran have a more complex phenomenon than the monohull, because of the interaction between the main hull and the side hull, which causes interference caused by changes in flow velocity, pressure changes, and wave interactions generated by each hull. The objective of this study is to analyze the resistance of trimaran and pentamaran NPL-4b models with transom-symmetrical hull and separation distances, specifically S/L ratios of 0.2, 0.3, and 0.4. Since a more limited base of experience exists for multihull ships, experimental or numerical modeling techniques are essential for designers. Numeric investigations were conducted using Numeca software, and experiments were performed in a towing tank. Both methods follow ITTC procedures. Furthermore, the numerical analysis with CFD simulation modifies the Navier-Stokes equation using the turbulence model k-ω SST to generate the RANS equation so that unsteady fluid flow problems can be calculated. It can be implemented in predicting resistance in Froude numbers (Fr) 0.2 to 0.6 at the systematic series of trimaran and pentamaran hull shapes at the model scale. The simulation results were compared to experimental data to validate the resistance of the ships. Overall, good resistance was produced by the trimaran and pentamaran in the C configuration at an S/L ratio of 0.4 with a total resistance coefficient C_T of 6.60 x 10^{-3} and 7.37 x 10^{-3}, respectively. The two results are in good agreement, both methods have a discrepancy of 3.70 %. Fluctuations influence the resistance in the wetted surface area (WSA), wave interactions between hulls, ship velocity, and wave propagation in the aft hull.

1. Introduction

The requirements for faster sea transportation have continued to increase in the areas of military and commercial applications. A new vessel should be designed to operate at the required speed with minimal power requirements [1]. This can be achieved by enhancing ship hull design and transitioning from monohull to multihull vessels, such as catamarans, trimarans, and pentamarans. Multihulls composed of center and smaller side hulls, are designed to reduce resistance on multihull ships. The

* Corresponding author.
E-mail address: kutama@its.ac.id (I Ketut Aria Pria Utama)

https://doi.org/10.37934/cfdl.17.3.5276

slender shape of the hulls allows them to exploit wave interference between the hulls and minimize wave-making resistance conducted by Peng [2]. Multihull ships have the advantages of large internal volume, large deck area, good transverse stability [3], and a wide range of possibilities for reducing wave resistance by exploiting the arrangement of hull elements [4] and varying hull shapes [5].

Using monohull and multihull ships for passenger ferries experiences varying resistance levels. Monohull ships produce more drag than multihull ships at high speed, one was conducted by Seif and Amini [6]. However, certain conditions and speeds may be better for monohulls than multihulls, see Utama *et al.,* [7]. Nasirudin *et al.,* [8] performed hull form optimization tests on a hard-chine monohull using two different bow shapes, namely a conventional bow and an inverted bow, and found that the average total resistance reduction of the inverted bow was about 5% compared to the conventional bow. The catamarans are a popular type of multihull ship. Catamarans exhibit a distinct hydrodynamic phenomenon known as viscous and wave interactions between the demihulls. According to Utama *et al.,* [9], the interference resistance between two ship hulls caused the otherwise symmetrical water flow around the demihull to become asymmetrical. The viscous interference factor β can determine the hull interference on a catamaran. Suastika *et al.,* [10] designed the foil system lifted the vessel and reduced its wetted surface area, this system impacts the running sinkage and trim and lowers the height of waves (wash) at high speeds, resulting in reduced wave-making resistance by 32%.

Although the catamaran has effectively minimized ship resistance for decades, the fast ferry industry and navies still require unique hull forms that offer significantly more deck space and are capable of operating at higher speeds than conventional hull forms. A trimaran is a form of multihull ship that can meet these requirements. It has two side hulls on both sides of the center hull, which can reduce ship resistance, Yildiz *et al.,* [11] conducted tests on a single outrigger configuration across a range of speeds up to a Froude number of 0.5. Nine different outrigger configurations were tested, and the resulting wave profile on the center-hull and wave patterns clearly showed the impact of interference between the center-hull and outriggers on the calculated resistance. The trimaran creates a wider Wetted Surface Area (WSA) than conventional hull forms, where WSA increases frictional resistance at low speed. Nevertheless, at high speeds, the slender hull form of a trimaran provides less wave-making resistance [12]. The multihull concept, known for its potential for low resistance at high speeds, is the subject of ongoing research. Previous research conducted by Yuliora *et al.,* [4] has explored various trimaran design configurations at five-speed variations utilizing computational numerical formulations, and it was found that the maximum S/L ratio of 0.4 provides a practical C_T value, especially at Fr 0.6. This is in line with research by Utama *et al.,* [13], where the Interference Factor (IF) of trimaran at separation distances position with S/L 0.4 is lower than at S/L 0.3.

The relative positioning of sidehulls to the mainhull is identified as a critical factor influencing multihull performance, with sensitivity to separation distances and the potential for minimizing wave resistance through shape modifications. The Pentamaran is a type of multihull ship that has recently been developed, with a structure consisting of a main hull and four side hulls that can provide stability. Therefore, it is necessary to analyze the pentamaran hull resistance to find out how effective the hull is compared to other multihull hulls. According to Dudson and Gee [14], pentamaran ships exhibit superior stability and seakeeping abilities while offering a more expansive deck space when compared to monohull ships of the same displacement. Numerous studies have been conducted to determine the optimal configuration of pentamarans. The Wigley hull form pentamaran model was investigated by Yanuar *et al.,* [15] to achieve this goal. Five asymmetric and symmetric hull configurations were examined, with the symmetric configuration experiencing constructive and destructive interferences in three separation variations, ultimately resulting in stabilization. Yanuar

et al., [16] assessed the destructive effects caused by wave interference troughs of trimaran and pentamaran with variation transom and non-transom on aft-hull, with experimental methods. Sulistyawati *et al.,* [17] using Michell's theory, compute various pentamaran configurations and compare the results with Yanuar *et al.,* [16] data, considering interference flow around the hulls. The results are consistent with Michell's theory, especially at higher speeds. This validates the usefulness of theoretical predictions, even when accounting for viscous factors at lower speeds.

The development of fast digital computers and accurate numerical algorithms has caused a revolution in the study of fluid dynamics, specifically Computational Fluid Dynamics (CFD). With CFD, analyzing a model with high precision is possible, but it requires a large amount of computer memory. Nonetheless, the method is affordable, accurate, and has a short duration, according to Andersson *et al.,* [18]. Furthermore, Nazemian and Ghadimi [19] conducted a CFD simulation to investigate the optimization of the trimaran hull shape. They applied the CFD software StarCCM+ to predict resistance for the optimization of the trimaran side hull arrangement. The results demonstrated a reduction in resistance of 6.9%.

CFD is particularly useful in analyzing flows around complex geometries where experimental measurements might be challenging. However, the accuracy of CFD in predicting these complex flows needs to be validated against experimental data. In summary, experimental methods serve as a crucial validation tool for CFD simulations by providing visualization of real data for direct comparison, ensuring the accuracy and reliability of the computational models. The synergy between experimental and numerical approaches enhances the overall understanding of fluid dynamics and supports the development of more robust simulation methodologies. Riyadi and Suastika's research [20] indicates that CFD simulations accurately capture the physical phenomena observed during the towing test, where CFD was able to provide detailed visualization of the wave patterns and the locally high water overflow near the bow. Additionally, Ahmed and El-Ela [21] conducted an initial numerical analysis to create the DTMB 5415-51 ship model, the validation of the model was followed by a comparison with experimental results obtained from a towing tank to confirm its resistance.

The research addresses the contemporary demand for high-speed and fuel-efficient ships, emphasizing sustainability in the maritime industry. Exploring novel hull configurations like trimarans and pentamarans, known for their potential to reduce ship resistance due to their odd number of hulls as proved by Yanuar *et al.,* [22] and Wang *et al.,* [23], the study investigates the hydrodynamic advantages of these multihull designs. The complex hydrodynamic challenge introduced by the interaction between the mainhull and sidehulls is a focal point, emphasizing the need to understand and quantify this complexity for optimizing hull shapes and configurations to minimize resistance.

This study employs a comprehensive approach by integrating numerical and experimental analysis. The numerical method utilizes CFD simulation with Numeca software, using the unsteady RANS approach and the k-ω SST turbulence model. The CFD simulation results have been validated with several parameters: grid independence study, convergence study, y^+ value verification, and numerical uncertainty analysis. The CFD results were validated with the EFD results on the towing tank belonging to ITS Surabaya. This dual methodology follows ITTC formulas, standards, procedures, guidelines, and recommendations, thereby increasing the overall reliability of the study. The ship model was tested in calm water with Fr variations of 0.2 to 0.6 and S/L variations of 0.2 to 0.4, each with an interval of 0.1. This study demonstrates the direct impact of separation distance on trimaran and pentamaran resistance using the transom-symmetric NPL-4b series hull, especially analyzing and visualizing CFD and EFD results. Furthermore, this study discusses the composition of total resistance components, such as the wave resistance coefficient C_W, the friction resistance coefficient C_F, and the viscous pressure resistance coefficient C_{VP}. The last information gained from this research has practical implications for reducing drag and hydrodynamic complexity in trimarans and pentamarans.

2. Methodology

2.1 Hull Geometry Specification

The flow around the trimaran and pentamaran hull was simulated on a model scale. The length of the waterline (L_{WL}) of the trimaran sidehull is established as half of the length of the mainhull. While the displacement of the pentamaran sidehull is equal to half of the displacement of the trimaran sidehull, this is done to ensure equal displacement. The NPL 4b series hull type was used for the model data, with an L/B ratio of 9 and a B/T ratio of 2 [24], as presented in Table 1.

Table 1
General particulars of the trimaran and pentamaran

Main feature	Symbol	Unit	Mainhull	Sidehull Trimaran	Sidehull Pentamaran
Length of water line	L_{WL}	m	0.800	0.400	0.272
Breadth	B	m	0.090	0.045	0.035
Draught	T	m	0.045	0.022	0.019
Wetted Surface Area	WSA	m^2	0.054	0.014	0.012
Displacement	Δ	kg	1.285	0.160	0.080

The model's configuration is based on variations in separation distances (S/L ratio), which are similar to previous observations [4]. Table 2 depicts the positioning of the sidehull to the mainhull.

Table 2
The configurations of trimaran and pentamaran models

S/L	S (m)	Symbol
0.2	0.16	A
0.3	0.24	B
0.4	0.32	C

An illustration depicting the separation distance settings for trimaran (T) and pentamaran (P) can be observed in Figure 1.

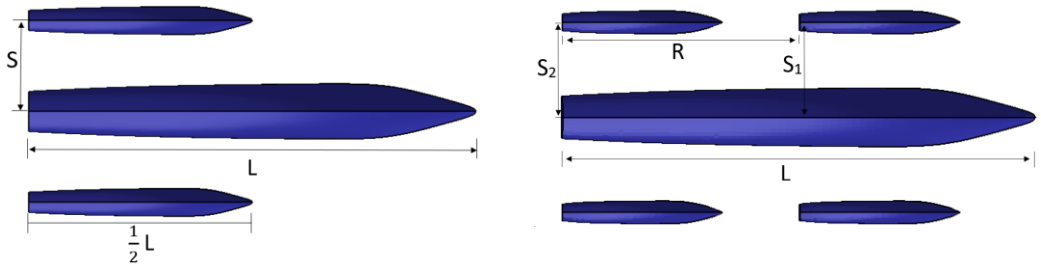

(a) (b)

Fig. 1. Separation distances position (a) Trimaran and (b) Pentamaran

In Figure 1, symbols S, S_1, and S_2 are equivalent, and R has a value of 0.4 meters or ½ L and L = L_{WL}. The scale used in the model is 1: 62.5 with configuration variations based on the S/L ratio, as shown in Figure 2.

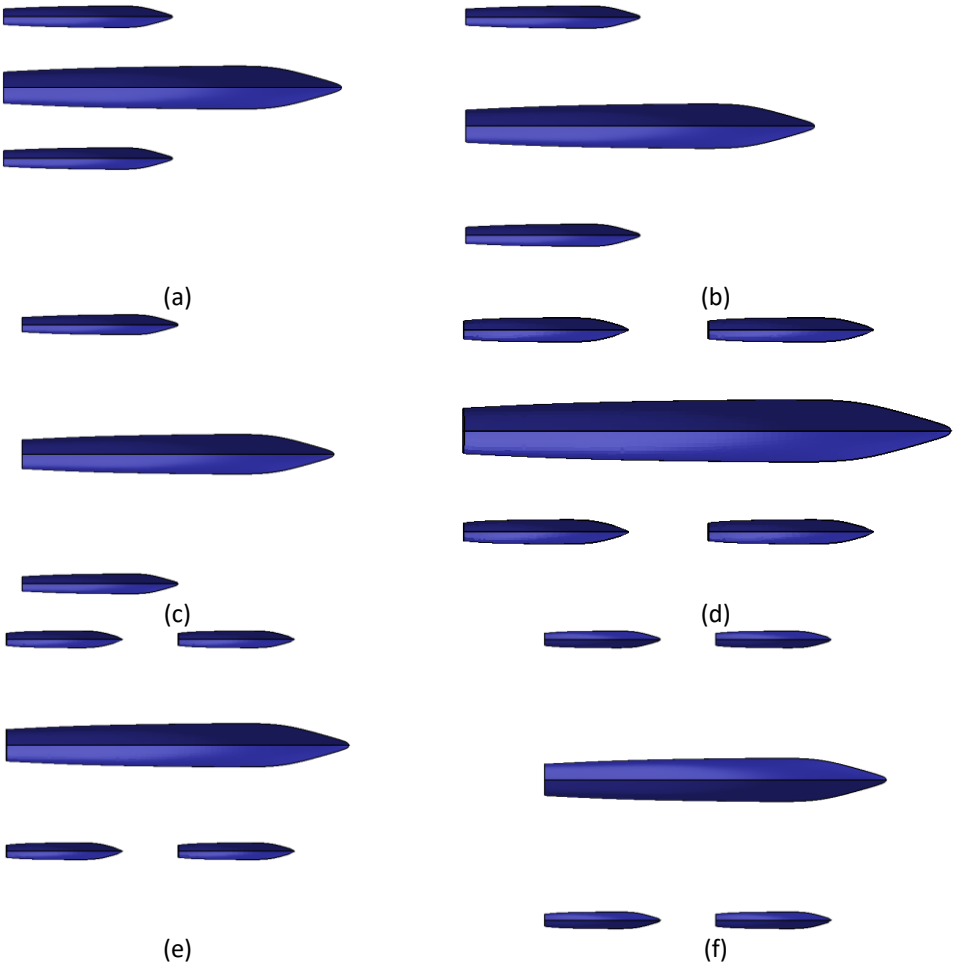

Fig. 2. Trimaran and Pentamaran hull configurations (a) T-A, S/L=0.2 (b) T-B, S/L=0.3 (c) T-C, S/L=0.4 (d) P-A, S/L=0.2 (e) P-B, S/L=0.3 (f) P-C, S/L=0.4

The blockage effect relates to the influence of tank boundaries and model dimension on the accuracy of the resistance prediction so a blockage correction is necessary. This study utilized the blockage correction formulations of the Tamura blockage correction from ITTC Procedure 7.5-02-02-01 [25]. For the model with S/L ratio of 0.4 and at Fr 0.4, an ΔV/V blockage correction of 0.058 % was obtained, consistent with the study of Srinakaew *et al.,* [26]. This result is far too small; blockage correction is not applied to all the experimental data.

2.2 Prediction of Resistance

Several factors influence the durability of multihull ships, such as the shape of the hull, as in a study conducted by Fitriadhy *et al.,* [27] by optimizing a catamaran hull. Furthermore, the hydrodynamic interaction factor between the hulls is as done by Waskito *et al.,* [28] for trimarans. Yuliora *et al.,* [4] conducted a study of the influence of separation distance, speed, and Froude number on trimaran resistance then the scale effect factor as did Royce *et al.,* [29], Wang *et al.,* conducted a study of trimaran wave interference [23], trimaran model optimization techniques by Zhang *et al.,* [30], and finally experimental testing of pentamaran in the study of Yanuar *et al.,* [31]. When a vessel travels at a consistent velocity in calm waters, it encounters opposition from the friction between the hull and water. Additionally, the vessel expends energy to generate water waves as it passes through a fluid that forms a boundary layer, a thin layer attached to the hull surface. Due to the velocity gradient across the boundary layer, the fluid will shift, and the object experiences

resistance in the tangential direction, called frictional resistance (R_F). The frictional resistance of multihull ships depends on the wetted surface area (WSA) and the Reynolds numbers (Re). Viscous form resistance is evaluated from the form factor (1+k). The effect of viscosity causes both frictional resistance and viscous form resistance. The Froude hypothesis separates the total resistance into two components, namely frictional resistance and residual resistance (R_R). Residual resistance by definition, is obtained by subtracting the total resistance from the friction resistance. This residual resistance includes wave-making resistance (R_W) and viscosity (viscous resistance R_V). Ship resistance can be expressed as the coefficient of total resistance (C_T) Eq. (1).

$$C_T = \frac{R_T}{\frac{1}{2}\rho v^2 (WSA)} \tag{1}$$

To calculate the coefficient of friction resistance (C_F) and coefficient of pressure resistance (C_P) refer to Eq. (2) and Eq. (3).

$$C_F = \frac{R_F}{\frac{1}{2}\rho v^2 (WSA)} \tag{2}$$

$$C_P = \frac{R_P}{\frac{1}{2}\rho v^2 (WSA)} \tag{3}$$

R_T is the total resistance, R_F is the friction resistance and R_P is the pressure resistance. The resistance coefficient is a dimensionless parameter to measure a ship's resistance as it travels through water. It is influenced by ship resistance, fluid density (ρ), wetted surface area (WSA), and speed (v^2).

Besides the C_F and C_P components, several other ship resistance components affect the coefficient of total resistance, such as the coefficient of viscous resistance (C_V), coefficient of wave resistance (C_W), and coefficient of viscous pressure resistance (C_{VP}), using Eq. (4), Eq. (5), and Eq. (6), respectively.

$$C_V = (1 + k)\, C_F \; ; \quad (1+k) \text{ is form factor} \tag{4}$$

$$C_W = C_T - C_V \tag{5}$$

$$C_{VP} = C_V - C_F \tag{6}$$

Further detail of Eq. (6) can be seen in Molland *et al.,* [32].

The coefficient of total resistance on the non-interference trimaran hull (unbonded) $C_{T_{tri-NI}}$ and interference (bonded) $C_{T_{tri-IF}}$ can be calculated by Eq. (7) and Eq. (8), respectively.

$$C_{T_{NI}} = C_{T_{MH}} + 2C_{T_{SH}} \tag{7}$$

$$C_{T_{IF}} = C_{T_{NI}} + +\Delta C_T \tag{8}$$

With $C_{T_{MH}}$ the coefficient of total resistance on the mainhull, $C_{T_{SH}}$ total resistance coefficient on the sidehull trimaran or pentamaran, and the difference in resistance coefficients between non-interference and interference is denoted by ΔC_T for trimaran or pentamaran designs. Evaluation of the calculated hydrodynamic interference effect for each configuration can be determined through

the interference factor (IF) parameter. IF is calculated as the difference in total resistance between three separate hulls and one bonded trimaran hull while easily expressing the difference as a ratio of total resistance non-interference using Eq. (9).

$$IF = \frac{C_{T_{tri-IF}}}{C_{T_{tri-NI}}} - 1 \tag{9}$$

the fluctuation of the interference factor is proportional to the fluctuation of the total resistance coefficient, where the smaller the C_T, the smaller the IF, which has been proven by Hafez and El-Kot [33], and Yanuar *et al.,* [22].

2.3 Numerical Setup
2.3.1 Governing equation

The Reynolds-Averaged Navier-Stokes (RANS) equation encapsulates the key principles of conserving mass, momentum, and energy when simulating turbulent flows through Computational Fluid Dynamics (CFD). The conservation laws are usually expressed in three distinct mathematical equations, but for this specific study, the energy equation is excluded. The RANS equations for Newton's incompressible viscous fluid are expressed as Eq. (10) – (11), found in reference [34]. The initial equation pertains to the continuity equation.

$$\nabla.[\rho U] = 0 \tag{10}$$

Momentum equation,

$$\frac{\partial}{\partial t}[\rho U] + \nabla.\{\rho U\mathbf{U}\} = -\nabla P + [\nabla.\{\bar{\tau}_{ij} - \rho\overline{\mathbf{u}'u'}\}] + \rho g \tag{11}$$

In Eq. (11) there is an additional term in the form of the divergence of the viscous stress, namely $-\rho\overline{\mathbf{u}'u'}$, and is given the notation τ^R (Reynolds stress). For incompressible flow, τ^R is defined in Eq. (12).

$$\tau^R = -\rho\overline{\mathbf{u}'u'} = \mu_t\{\nabla\mathbf{U} + (\nabla\mathbf{U})^T\} - \frac{2}{3}(\rho k)\,\mathbf{I} \tag{12}$$

μ_t is the turbulent viscosity and k is the kinetic energy of turbulence.

Turbulence modeling is a computational process utilized for calculating Reynolds stress and solving systems of Eq. (10) – (11). In the k-ω SST model, Menter [34] made modifications to the turbulent viscosity μt by constraining its value using Eq. (13) to derive the equations for Eq. (12) and ultimately Eq. (11).

$$\mu_t = \frac{\rho a_1 k}{\mathrm{Max}\left(a_1\omega, \sqrt{2}S_t F_2\right)} \tag{13}$$

With a_1 = 0.31, S_t is strain rate magnitude and F_2 = tanh (γ_2^2). In this study, it is modeled using free surface modeling.

2.3.2 Boundary conditions and meshing

The selection of boundary conditions and domain dimensions is adjusted to the selected problem estimate. The specified boundary conditions include a moving hull body with a no-slip condition imposed on the hull surface, improved: The surfaces have been subjected to the free-slip condition, which is applied to the opening, bottom, and side walls. The hull center plane or mirror is a symmetry condition; the flow velocity at the inlet is set as the tested speed; the outlet defined as hydrostatic pressure is defined as a function of water level height. Additionally, the initial position of the free surface is determined by defining the volume fraction function of the water and air at both the inlet and outlet. the trimaran model on a model scale with a scale of 1: 62.5 from the actual size, the boundary conditions are set for freshwater with a temperature of 28° C which has a density of water (ρ) of 996.236 kg/m^3, The mass density and viscosity of water are determined according to the ITTC Procedure 7.5-02-01-03 [35]. The specifics of boundary conditions and domain dimensions are stated in Figure 3.

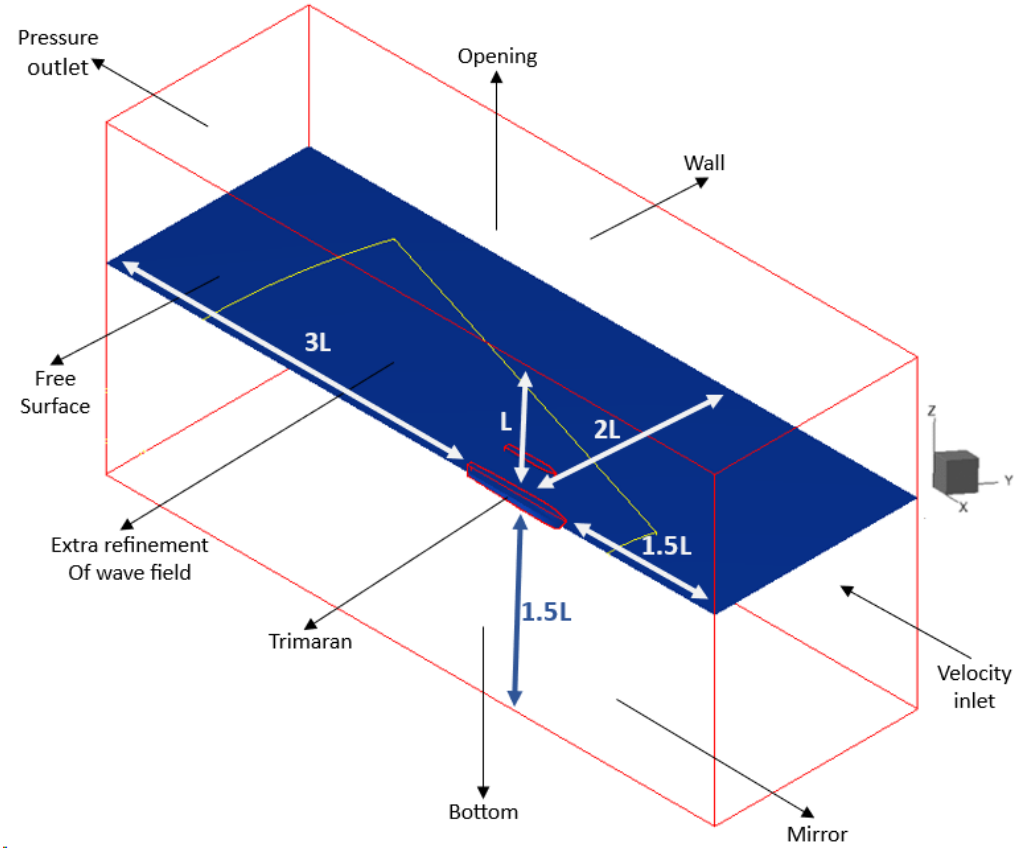

Fig. 3. Domain dimensions and boundary conditions

In this case, the mesh generation is carried out using the Hexpress module. First, import geometry from the CAD model, prepare geometry so that the geometry is clean, define regions and boundaries, and choose the type of mesh want to generate. In this study, the structured type was chosen (Figure 4(a)). Structured meshes typically consist of orthogonal quadrilateral (2D) or hexahedral (3D) elements. This type of mesh allows for easy node enumeration and access to adjacent elements or nodes without requiring connectivity information [36] (Figure 4(b)). Additionally, coordinates can be accessed easily due to the consistent size of each element (Figure 4(c)). So, they are suitable for complex geometry and require a higher resolution mesh. Second, a mesh quality check is done to

ensure that the mesh meets predefined criteria, and mesh refinement is done to improve resolution (Figure 4(d)). Stages that are no less important are defining boundary conditions within the mesh and then exporting the mesh in a format compatible with Numeca's CFD solvers.

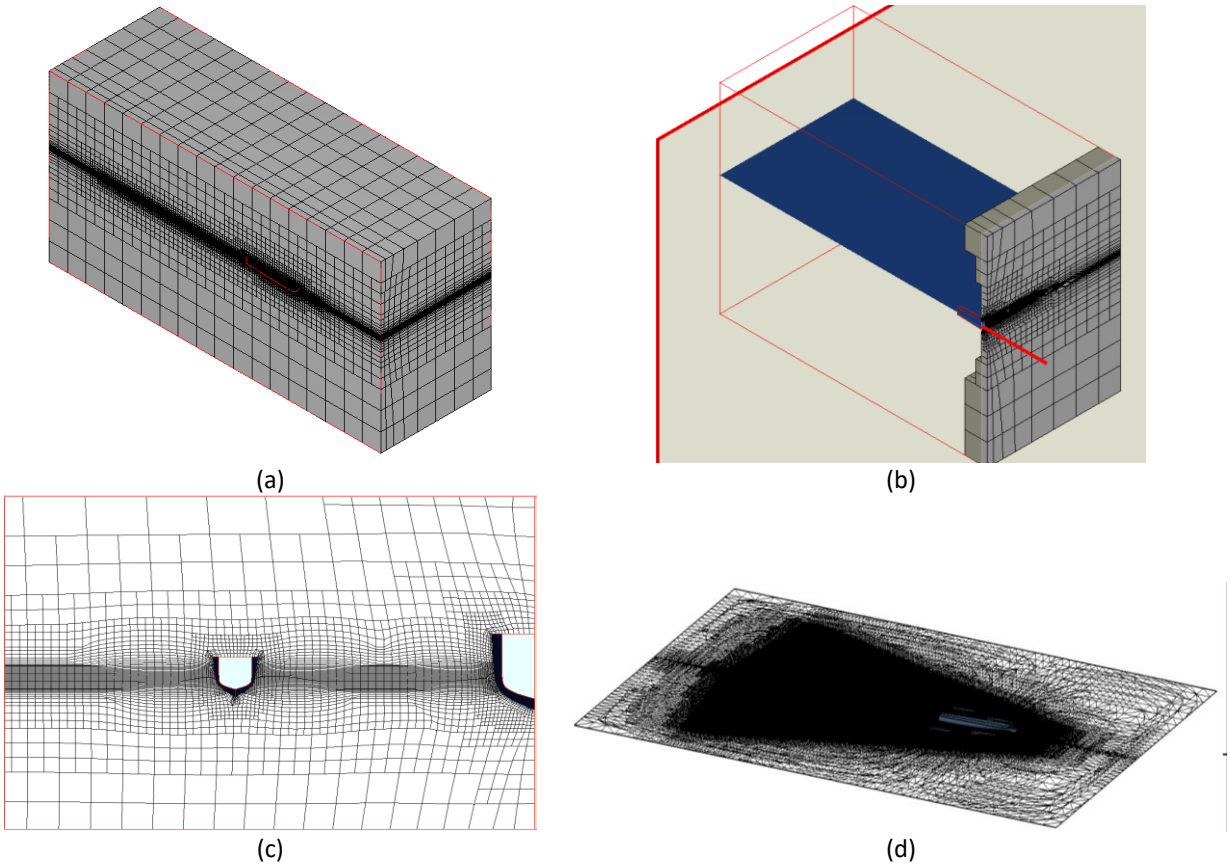

Fig. 4. Grid resolution in the meshing process (a) Structure mesh (b). Grid Generation (c) Grig topology (d) Extra refinement of the wave field

2.3.3 Grid independence study

The quality or quantity of the grid mesh is fundamental to this CFD simulation convergence and accuracy [37]. According to the Molland and Utama [38], the grid independence reaches the optimum position if the difference resistance between several elements and the previous element is less than 2% In. Table 3 and Table 4 show the discrepancy of each configuration in grid independence in detail and plotted in Figures 5(a) and 5(b).

Table 3
Grid independence Trimaran

Run	T-A		T-B		T-C	
	C_T x 10^3	ΔC_T (T-A) (%)	C_T x 10^3	ΔC_T (T-B) (%)	C_T x 10^3	ΔC_T (T-C) (%)
1	7.93	-	7.64	-	7.60	-
2	7.49	5.88	7.22	5.72	7.06	7.52
3	7.03	6.54	6.75	7.01	6.65	6.28
4	6.91	1.64	6.68	1.07	6.60	0.74
5	6.81	1.47	6.61	1.00	6.56	0.59

Table 4
Grid independence Pentamaran

Run	P-A		P-B		P-C	
	$C_T \times 10^3$	ΔC_T (P-A) (%)	$C_T \times 10^3$	ΔC_T (P-B) (%)	$C_T \times 10^3$	ΔC_T (P-C) (%)
1	8.66	-	8.50	-	8.68	-
2	7.99	8.43	7.92	7.35	8.08	7.05
3	7.67	4.11	7.58	4.47	7.87	4.00
4	7.59	1.08	7.50	1.04	7.82	0.65
5	7.52	0.97	7.49	0.19	7.81	0.58

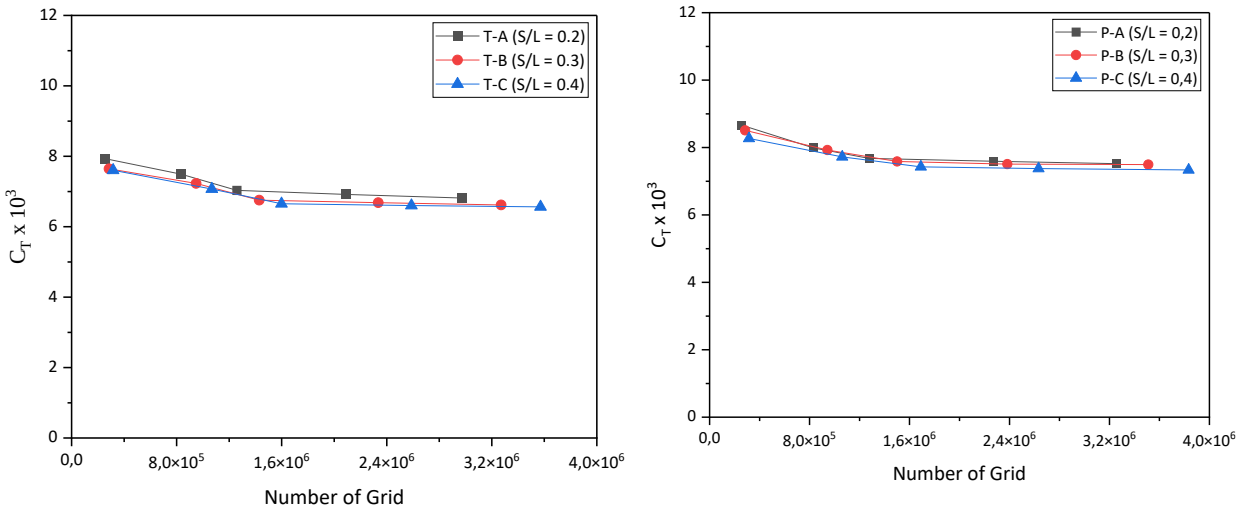

(a) (b)

Fig. 5. The graph of the grid independence (a) Trimaran and (b) Pentamaran models

Figure 5 shows that the greater the ratio of S/L, the greater the number of grids produced with the same surface refinement composition, so it can be said that the greater the ratio of S/L, the greater the number of grids needed to reach the grid independence. In this study the number of mesh elements or grid 2,093,216 for the T-A model is quite optimal and accurate, where the number of elements used in the computing shows that the condition that is grid independence C_T does not change significantly again, meaning that the number of grids is effective enough to reduce computing cost and time. The effective number of grids for T-B and T-C respectively is 2,335,416 and 2,587,968 grids, and the illustration can be seen in Figure 5(a). The same thing applies to the pentamaran grid, the effective number of grids for P-A, P-B, and P-C are 2,271,572, 2,382,671, and 2,633,111 grids, respectively in Figure 5(b).

2.3.4 Verification of y^+

Verification of y^+ is required to generate a reasonable-quality grid for the turbulent flow model. The y^+ value corresponds to the first node nearest the wall, known as y_1^+ ($y_1^+ = \rho U_\tau Y y_{wall}/\mu$). Therefore, for the model scale (equivalent to low-Re), y^+ should range from 30-50, whereas for high-Re it should be between 50 and 300. Low Reynolds number modeling is suitable for the viscous sublayer and accurately predicts flow conditions for $y_1^+ < 1$. In contrast, the high Reynolds number model employs an analytical function in the log-layer and is a better fit for y_1^+ in the range of 30 to 300. For wall function boundary conditions, $y_1^+ > 30$ is acceptable, while no-slip conditions are recommended for $y_1^+ < 1$ [39]. The present study explores values of y^+ ranging from 48 to 56, as shown in Table 5.

Table 5
Range of y+ values at C configurations

Fr	T-C		P-C	
	y^+ (min)	y^+ (max)	y^+ (min)	y^+ (max)
0.2	0.09	43.87	0.01	55.98
0.3	0.03	54.46	0.05	54.22
0.4	0.05	46.95	0.14	46.86
0.5	0.23	48.17	0.23	48.21
0.6	0.39	49.01	0.22	48.80

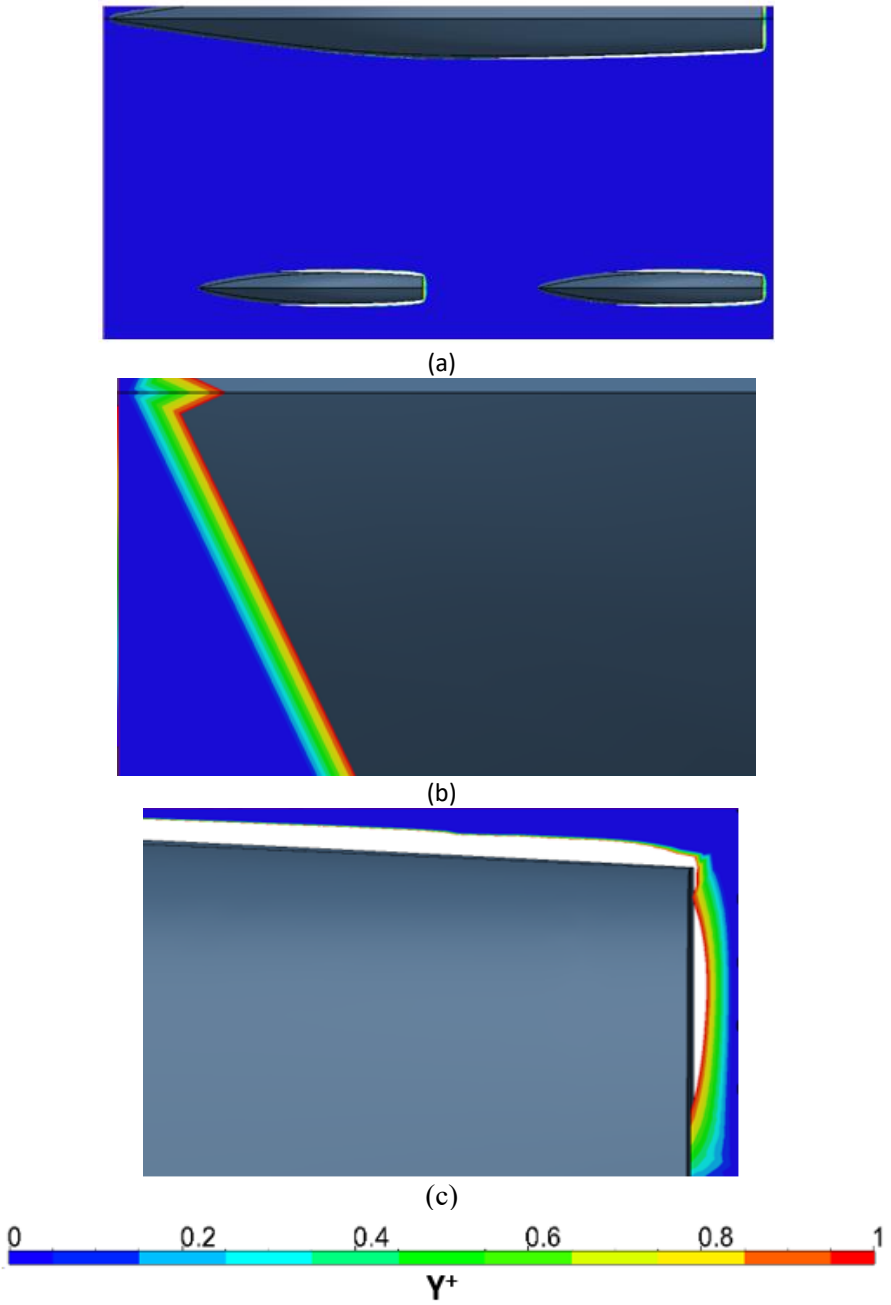

Fig. 6. The values of y^+ (a) y^+ value contour on the bottom of the starboard side (b) y^+ value contour on fore-hull (c) y^+ Value contour on aft-hull

2.4 Experimental Setup

The experiment was conducted in calm water following the guidelines of the International Towing Tank Conference (ITTC) 1978 for analyzing ship resistance components. A towing tank test is conducted in a tank measuring 50 m x 3 m x 2 m using an electric motor. The model is mounted with a load cell transducer and connected to an acquisition data system to determine the model resistance value, depicted by the strip chart recorder. Schematically it can be seen in Figure 7.

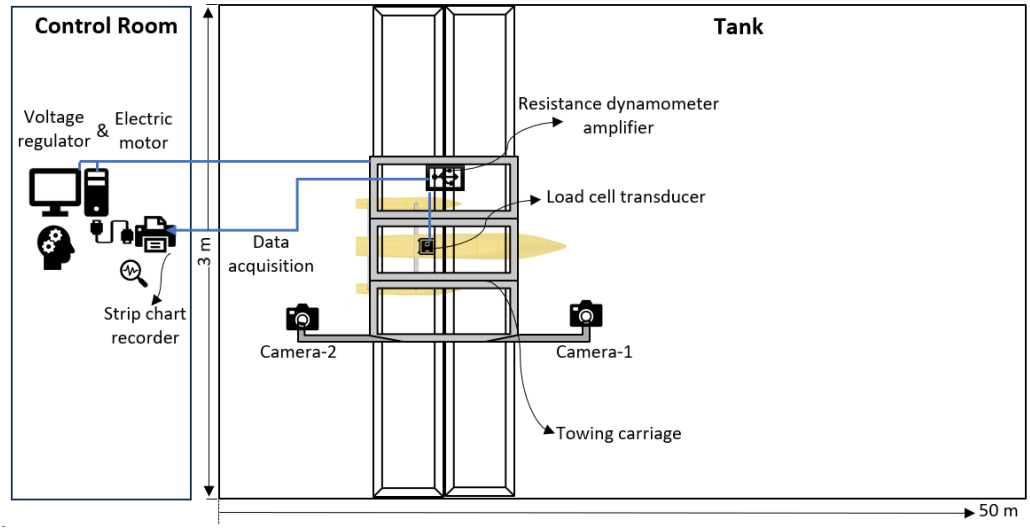

Fig. 7. Top plane of the towing tank arrangement

Figure 8 shows a photo of the model in the towing tank in detail.

Fig. 8. Pentamaran Model in towing tank

The physical model of both the trimaran and pentamaran were constructed in a similar size, shape, and configuration to the CFD simulation model data, with a fiberglass base material using a three-dimensional printed mold. This towing carriage is powered by four electric motors. The speed of the electric motor is determined by the applied voltage. The laboratory's electrical measurements and calibration results demonstrate that a voltage of 2.5 volts applied to the motor will cause the towing carriage to move at a speed of 1 m/s. The tests were conducted at Fr 0.2 to 0.6, so a 0.7 Volt range from 1.4 to 4.2 Volts is necessary to operate the motor. The strip chart recorder records results

that are presented as a deviation graph with peaks and valleys. Calculation of curve deviation values at all peak and valley points provides the total resistance.

2.5 Verification and Validation (V & V) Study

2.5.1 Uncertainty analysis in CFD V & V

In this research, the grid Convergence study is employed as a means of verification. Convergence studies were conducted using three different mesh resolutions: coarse, medium, and fine. The inflation layer remained constant during the entire analysis because the mesh resolution is based on standard wall calculations, as given in Table 6.

Table 6
The mesh resolution details for T-A

Parameter	Fine (1)	Medium (2)	Coarse (3)
Face sizing (m)	0.04	0.055	0.065
Number of Cells (NC)	2,701,110	1,483,959	884,680
Total resistance coefficient ($x10^{-3}$) (C_T)	6.622	6.659	6.801

To estimate errors and uncertainties for monotonic convergence ($0 < R_i < 1$), we apply generalized Richardson extrapolation. Results show several oscillations for the convergence of oscillations ($R_i < 1$). However, for divergence ($R_i > 1$), the results are different and the error and uncertainty cannot be determined (Ri is the convergence ratio). To report the quality of grid convergence, the grid convergence index (GCI) is a standard method. Which is calculated at the refinement step. The GCI is calculated for stages from grid 3 to 2, and from 2 to 1, where e is the error between the two grids and Fs is the safety factor (Fs=1.25). The recommended value for the refinement ratio r_i is $\sqrt{2}$.

The numerical uncertainty of the CFD model is based on the data in Table 6. To estimate the grid error, this paper uses the Richardson extrapolation method for grid convergence as done by Zingg *et al.,* [40], and Celik *et al.,* [41]*,* where the grid convergence study was performed based on the ITTC recommendations for uncertainty analysis [42]. The numerical uncertainty analysis is presented in Table 7.

Table 7
The numerical uncertainty analysis for T-A

Outcome	Equation	Value
Difference of estimation	$\varepsilon_{21}= C_{T2}-C_{T1}$	0.037
	$\varepsilon_{32}= C_{T3}-C_{T2}$	0.142
Refinement ration	$r_{21}= (NC_2/NC_1)^{1/3}= r_{32}= NC_3/NC_2^{1/3}$	1.3
Convergence ratio	$Ri= \varepsilon_{21}/ \varepsilon_{32}$	0.260
Order of accuracy	$P=\ln(\varepsilon_{32}/ \varepsilon_{21})/\ln(r_i)$	5.126
Extrapolated value	$C_{T,ext-21}=(((r_{21}^p)C_{T1})-C_{T2})/(r_{21}^p-1)$	6.659×10^{-3}
	$C_{T,ext-32}=(((r_{32}^p)C_{T2})-C_{T3})/(r_{32}^p-1)$	6.851×10^{-3}
Approximate relative error	$e_{a21}=\lvert(C_{T1}-C_{T2})/C_{T1}\rvert$	0.5 %
	$e_{a32}=\lvert(C_{T2}-C_{T3})/C_{T2}\rvert$	2.1 %
Extrapolated relative error	$e_{ext-21}=\lvert(C_{T,ext-21}-C_{T1})/C_{T,ext-21}\rvert$	0.5 %
	$e_{ext-32}=\lvert(C_{T,ext-32}-C_{T2})/C_{T,ext-32}\rvert$	2.8 %
Grid convergence index (GCI)	$CGI_{21}=(Fs\lvert e_{21}\rvert/C_{T1}) \times 100\%$	0.9 %
	$CGI_{32}=(Fs\lvert e_{32}\rvert/C_{T2}) \times 100\%$	3.6 %

Table 7 shows the extrapolated relative error ranging from 0.5 % to 2.8 %, with a convergence ratio of 0.26, and CGI_{fine} of 0.9 %. Despite this, the fine mesh was selected for the inquiry since it offers a superior level of precision to the simulation, thereby reducing the amount of error that is introduced throughout the investigation.

The results of the simulation, as presented in Table 7, indicate a simulation error (δ_S) of 0.5%. This value is employed to compute the validation uncertainty (U_V) through the CFD validation procedure at ITTC procedure 7.5-03-01-01, as delineated in Eq. (14).

$$U_V^2 = U_D^2 + U_{SN}^2 \tag{14}$$

The U_D is the experimental data uncertainty and the U_{SN} is the simulation uncertainty. The comparison error (E) is defined as the discrepancy between the observed data (D) and the simulated values (S), as illustrated in Eq. (15).

$$E = D - S = \delta_D - (\delta_{SM} - \delta_{SN}) \tag{15}$$

With δ_D is the experimental data error, δ_{SM} is the additive modeling, and δ_{SN} is the numerical error. By using Eq. (14) – (15), obtained Uv = ±0.561 and E = ±0.323 for the P-C model at Fr of 0.6, and validation is achieved if $|E| < UV$ [42].

2.5.2 Uncertainty analysis in EFD V & V

The dimensions of the towing tank must be reported, along with the results of any associated tests. It is recommended that the dimensions be large enough to avoid any wall effects or blockages. ITTC (7.5-02-02-01) [25] provides a formula for correcting blockages, one of which is the Tamura formula, as outlined in Eq. (16).

$$\frac{\Delta V}{V} = 0{,}67\ m \left[\frac{L}{B}\right]^{\frac{3}{4}} \frac{1}{(1-Fr^2)}\ ;\ m = \frac{A_x}{A} \tag{16}$$

The maximum sectional area of the model is denoted by Ax, while the sectional area of the tank is designated by A. The length of the ship is expressed as L, while the breadth of the ship is represented by B. Finally, Fr denotes the Froude number. Table 8 presents verification of the blockage correction for each model and speed.

Table 8
The blockage correction

Fr	Blockage correction (%)					
	T-A	**P-A**	**T-B**	**P-B**	**T-C**	**P-C**
0.2	0.069	0.087	0.052	0.066	0.043	0.054
0.3	0.073	0.092	0.055	0.070	0.045	0.057
0.4	0.079	0.100	0.060	0.075	0.049	0.062
0.5	0.088	0.112	0.067	0.085	0.055	0.069
0.6	0.103	0.131	0.078	0.099	0.064	0.081

Table 8 illustrates that the blockage correction percentage is minimal, with an average of 0.093% for configuration A, 0.071% for configuration B, and 0.058% for configuration C. This indicates that the dimensions of the ship model for the towing tank are appropriate and do not influence the test

results. The results of the towing tank test or EFD can be validated through the use of uncertainty analysis. In this study, uncertainty analysis was conducted on the total resistance of the T-C model when Fr was 0.2 to 0.6. The total resistance data was obtained from repeated tests at each speed. As guided by ITTC recommendations (7.5-02-02-02) [43], and (7.5-02-02-02-01) [44], the results of the R_T uncertainty can be seen in Table 9.

Table 9
The uncertainty of R_T

Model	U_{RT} (%)				
T-C	Fr = 0.2	Fr = 0.3	Fr = 0.4	Fr = 0.5	Fr = 0.6
	±0.171	±0.163	±0.047	±0.074	±0.128

The mean R_T at all speeds is 779.65 N or 6.813 x 10^{-3} in C_T. The uncertainty in resistance for each speed is ±0.017, ±0.016, ±0.004, ±0.005, and ±0.008, respectively. The uncertainty in R_T is expressed in percent in Table 9, which presents the speed variations. Based on the data in tables 8 and 9 whose values are relatively small, the verification and validation of the EFD results are achieved. The methodology employed in this study is consistent with that employed by Park *et al.,* [45] in their research on the KVLCC2 ship. In this context, the standard uncertainty (U) is defined as the uncertainty due to measurements, expressed as the standard deviation (ISO, 1995) [46].

3. Results and Discussion

3.1 The Comparison of Trimaran and Pentamaran Resistance

The total resistance of the trimaran and pentamaran in C_T are shown in Figure 9. Configuration A, with an S/L ratio of 0.2 at low Fr, generates a smaller C_T than other configurations. However, for Fr values larger than 0.4, the increase in the S/L ratio is proportional to the decrease in C_T, this result is in line with the discussion by Yildiz *et al.,* [11] and Yanuar *et al.,* [47]. Overall, trimaran produces a smaller C_T than pentamaran, especially at Fr 0.3. It has an average discrepancy of 41.94%, the largest compared to other speeds, which is only 5-11% between trimaran and pentamaran. Each can be seen in Figure 9(a) and 9(b).

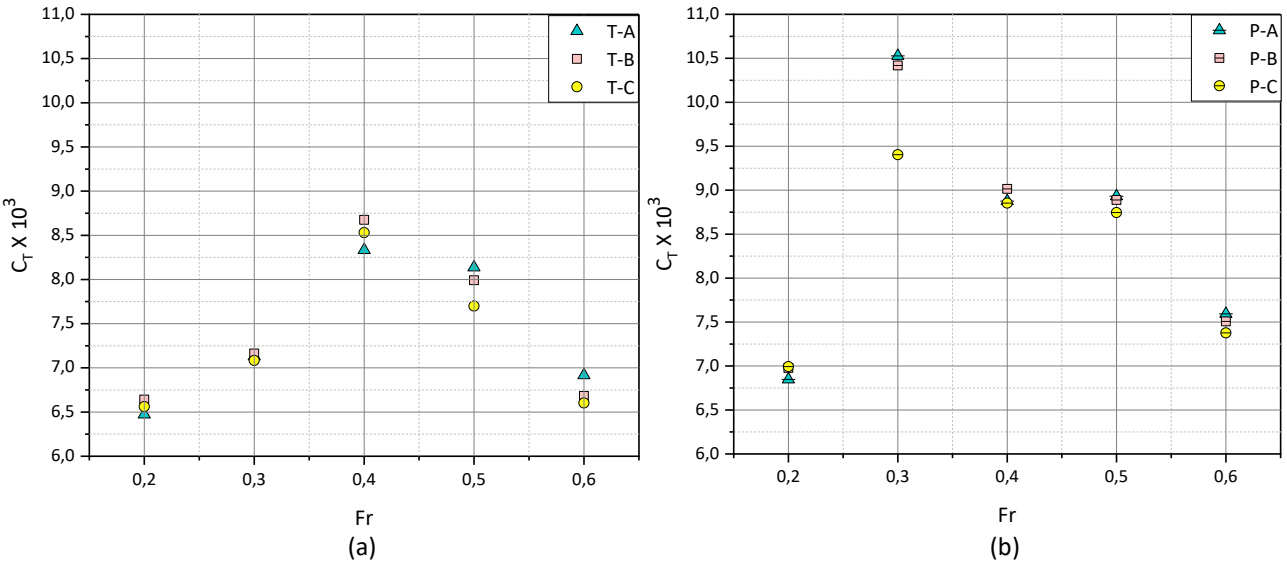

Fig. 9. The total resistance coefficient (a) Trimaran and (b) Pentamaran

Figure 9(a) shows an increase in C_T up to Fr 0.4, but it decreases again at Fr 0.5 to 0.6. This happens because when Fr 0.2-0.3, the wave has not yet formed, and the total resistance is dominated by friction resistance due to viscous factors, whereas at Fr 0.4, the wave has formed and dominates the total resistance. However, the decrease in C_T at Fr 0.5 to 0.6 is caused by wave interference, which occurs and results in cross-flow, which is increasingly away from the stern area of the trimaran. This indicated a reduction in the total resistance of the trimaran, which was discussed by Luhulima *et al.,* [48]. In contrast to the trimaran, Figure 9(b) shows an increase in the C_T of the pentamaran up to Fr 0.3, but it decreases slowly again at Fr 0.4 to 0.6. This occurs because, at Fr 0.3, waves have formed due to intense wave interactions between the hulls. Furthermore, waves with high pressure or energy are increasingly moving away from the stern area of the pentamaran, and this results in a decrease in C_T due to a decrease in C_W at Fr 0.5 to 0.6. This result is in line with research by Hu *et al.,* [49]. In more detail, Figure 10 shows the composition of the total resistance coefficient consisting of wave resistance, friction resistance, and viscous pressure resistance for each trimaran and pentamaran configuration.

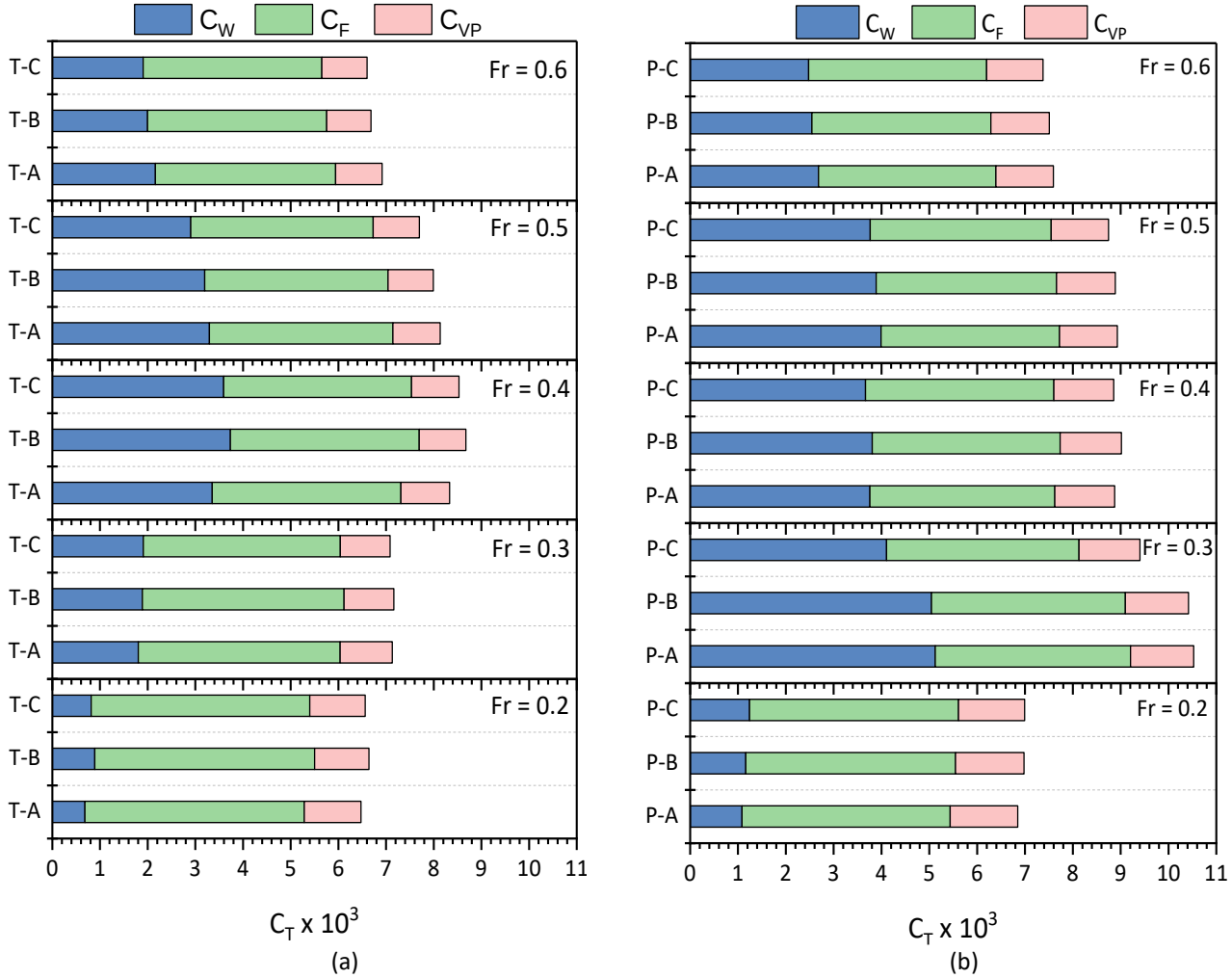

Fig. 10. The comparison of C_T components in each configuration (a) Trimaran and (b) Pentamaran

Figure 10(a) illustrates trimaran resistance, at Fr 0.2 C_W comprises only 12.13% C_T and is dominated by C_F at 70.15%. C_W proportionally increases until Fr 0.4 to 41.80% C_T, almost matching C_F at 46.45%. However, at Fr > 0.4, C_W proportionally drops to 29.99% C_T, once again dominated by C_F at 55.88%. C_{VP} composition remains stable at around 14.14% C_T under all conditions. Figure 10(b)

illustrates pentamaran resistance, at Fr 0.2 the composition of C_T is only 16.75%, dominated by C_F at 62.95%. As Fr increases to 0.3-0.5, C_W significantly increases to 44.24% C_T, almost the same composition as C_F, which is 42.16%. However, at Fr 0.6, C_W decreases to 34.27% C_T, dominated by C_F at 47.70%. The composition of C_{VP} remains stable in all conditions at around 15.41% C_T. The decrease in wave resistance at Fr > 0.5 is caused by the decreased impact of waves on each hull and the presence of wave breaking and spray. Some references, such as the study by Sulistyawati *et al.,* [17], analyzed the C_W and C_T components of a pentamaran ship. Du *et al.,* [50] conducted a rapid study of trimaran resistance estimation by describing the C_T and C_F components. Yildiz *et al.,* [11] carried out numerical and experimental studies on trimaran ships by considering the C_T and C_F components. Those three studies did not fully describe the resistance components, namely C_T, C_W, C_F, and C_{VP}. To address this gap in the literature, this study presents a comprehensive numerical and experimental investigation of trimaran and pentamaran resistance components.

3.2 Validation of Trimaran and Pentamaran Resistance

This section compares the experimental and numerical results under different speeds and separation distances, and the characteristics of the experimental and numerical results are discussed. The good agreement between the towing tank and CFD results enhances confidence in the numerical model's predictive capabilities. However, discrepancies may provide valuable insights for refining the simulation or understanding physical phenomena better.

A detailed explanation of the differences between the CFD and EFD results of the C_T trimaran and the pentamaran is given in Table 10.

Table 10
Discrepancy of the C_T on CFD and EFD results

Fr	ΔC_T (CFD – EFD) (%)					
	T-A	**T-B**	**T-C**	**P-A**	**P-B**	**P-C**
0.2	-3.627	-1.556	3.439	-4.080	-6.796	-5.576
0.3	-2.810	4.540	5.571	6.616	-3.524	-7.988
0.4	7.324	10.433	9.106	1.160	3.633	-3.774
0.5	5.963	8.711	8.682	5.259	6.715	5.255
0.6	4.910	7.625	6.797	2.555	1.856	4.578

The negative sign in Table 10 indicates that the EFD results are greater than the CFD results. An interesting phenomenon observed in Table 10 is the fluctuation of the difference between each model at each Fr. The trimaran at Fr = 0.4 exhibits the highest ΔC_T (CFD – EFD) among the other Fr, whereas on the pentamaran, the opposite occurs, with ΔC_T (CFD – EFD) shows the lowest value at Fr = 0.4. This phenomenon can be observed in Figure 10, which depicts the formation of a wave system at Fr = 0.4. It can be seen that the C_W component of the trimaran is highest at Fr = 0.4. Nevertheless, at the pentamaran, when Fr = 0.4, the wave system begins to decrease in amplitude, followed by a reduction in C_W. The total resistance calculation in the CFD method employs a fluid that has been calibrated following fluid property recommendations from ITTC [35], which remains constant under all conditions. In contrast, the EFD method permits alterations in fluid properties, such as those resulting from temperature changes, and a microscopic examination of the towing tank revealed the presence of a small quantity of material. The discrepancies in fluid properties between the CFD and EFD methodologies, when the wave elevation fluctuates, are such that it is not possible to avoid significant differences between the two methods.

Figure 11 describes the total resistance coefficients for the trimaran (T) and pentamaran (P) were measured with varying A, B, and C separation distances at Fr 0.2 to 0.6.

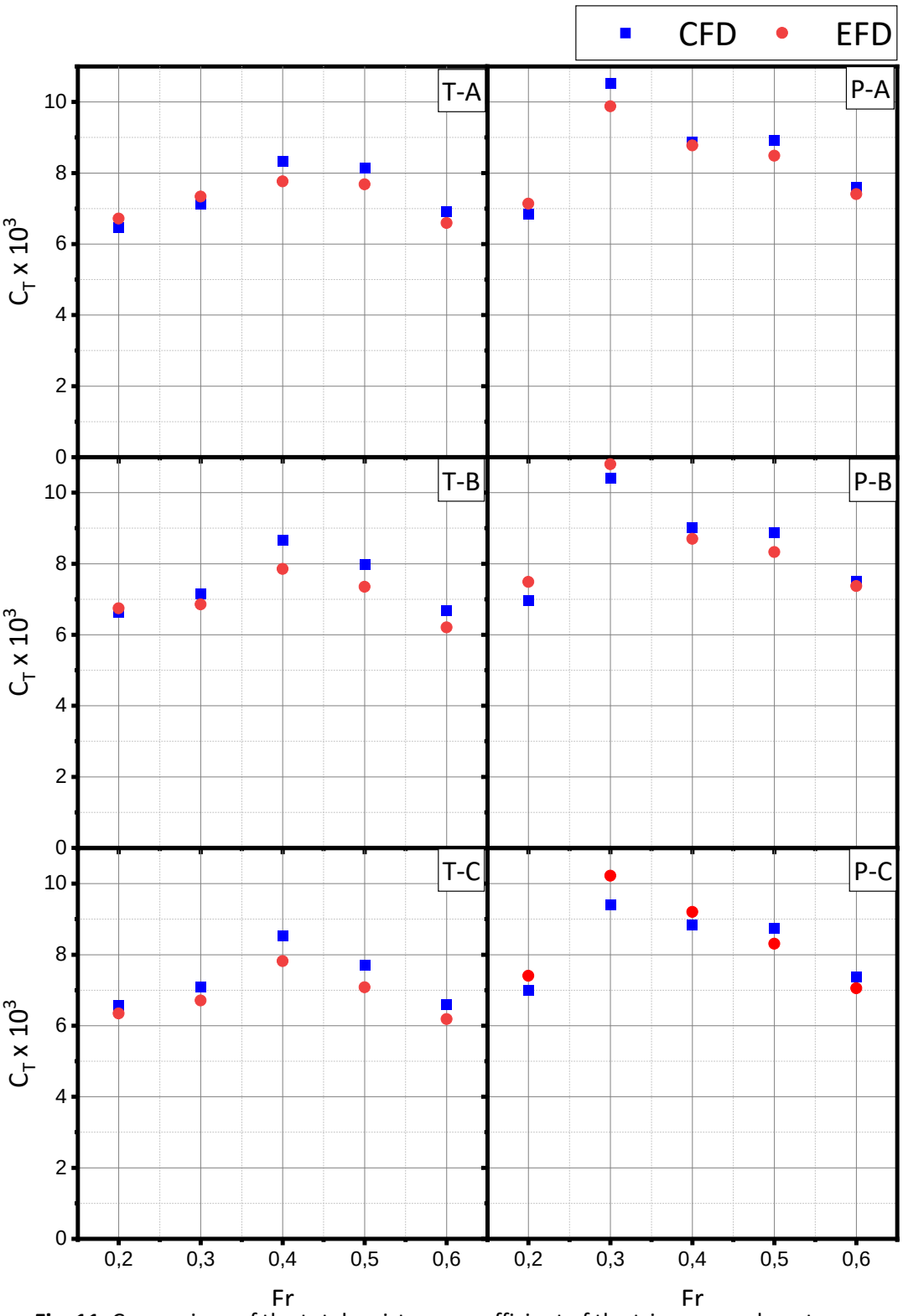

Fig. 11. Comparison of the total resistance coefficient of the trimaran and pentamaran in each condition

Figure 11 illustrates that the trimaran has a smaller C_T than the pentamaran, with an average discrepancy of 15.06%. It is important to note that there may be discrepancies between CFD and EFD results in certain C_T conditions, with an average difference of 3.70%. For example, in the T-A, T-B, and T-C configurations at Fr≥0.4, the CFD results consistently show a higher C_T than the EFD results. However, in the P-A and P-B configurations at Fr≥0.4, the EFD values tend to be smaller than the CFD results. In P-C, when Fr is less than 0.4, the C_T EFD results consistently show greater significance than the CFD results. This difference occurs because the fluid definition in the CFD simulation is close to the ideal fluid, incompressible, and inviscid. In contrast, during the experiment (EFD), the fluid was in actual fluid condition with various additional components. However, at the solver stage during the CFD simulation, the RANS equation with the k-ω SST turbulence model solves this problem approximately and exactly so that the fluid definition during the CFD simulation approaches the actual fluid conditions. When wave interference has a positive impact on reducing total resistance, especially at Fr ≥0.4, at that time, C_T EFD results tend to be smaller than CFD results. This is because, in these conditions, the average percentage of C_W is only around 36.22% from C_T, and C_F reaches 50.90% of C_T, so assuming inviscid fluid in the CFD simulation provides a greater C_F value representation than the C_F of EFD results, because inviscid fluids ignore viscosity, while C_F consists of viscous resistance and form factor.

3.2.1 Visualization of the trimaran wave patterns of the CFD and EFD results

Figure 12 shows a visualization of the CFD and EFD results of the wave patterns generated by each trimaran configuration at Fr 0.5.

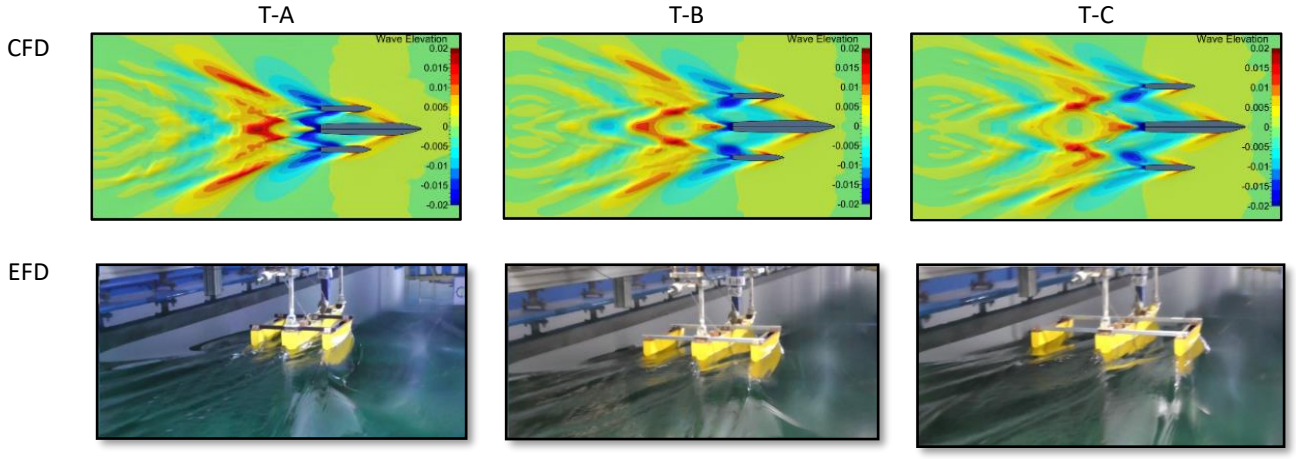

Fig. 12. Visualization of wave patterns created by a trimaran at Fr = 0.5

Figure 12 demonstrates that the distance between the trimaran hulls affects the wave pattern. The dominant dark blue and dark red colors on the stern and stern shoulders indicate a strong interaction (T-A). The CFD results are consistent with the image capture of the EFD process. A stern wave system is formed on the shoulder of the hull and at the stern of the T-C model, but it is not visible due to interference from the stern system itself. A stern wave system formed on the shoulder of the hull and at the stern of the T-C model, but it is not visible due to interference from the stern system itself. When approaching the divergent wave system, the crest line turns back and finally disappears in the divergent system, this aligns with Harvald's description [51]. The results of the EFD recordings show that as the distance between the hulls increases, the cross-flow is formed at the

stern, which moves further away. This leads to a decrease in wave resistance value because of the reduced influence of waves between the hulls and the occurrence of wave breaking and spray.

3.2.2 Visualization of the pentamaran wave patterns of the CFD and EFD results

Figure 13 shows a visualization of the CFD and EFD results of the wave patterns generated by each pentamaran configuration at Fr 0.5.

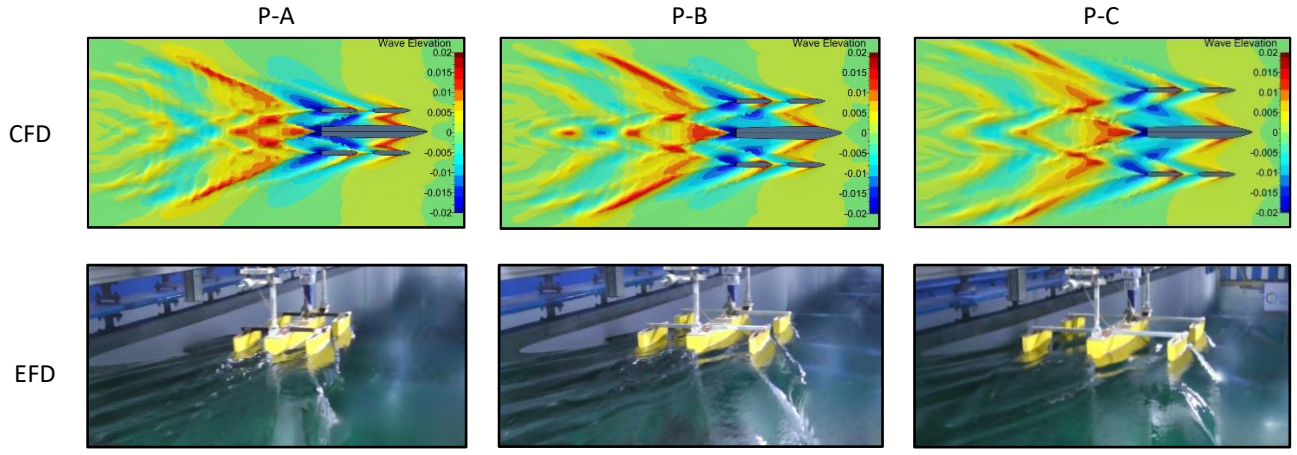

Fig. 13. Visualization of wave patterns created by a pentamaran at Fr = 0.5

The pentamaran model produces a trend similar to that of a trimaran regarding the effect of separation distance. However, in Figure 13, it can be observed that the meeting of the wave system from the sidehull with a tandem formation parallel to the mainhull (or vice versa) occurs cross flow, which produces a peak line that suddenly disappears in the next wave divergent system. This phenomenon occurs from the stern shoulder to the stern. This phenomenon has a significant interference impact on each hull, particularly the P-A model, which generates more significant pressure in the stern area than the P-B and P-C models. This is consistent with the results of EFD recordings, where cross-flow appears to form further from the stern as the separation distance increases.

3.3 Interference Effects

Interference is defined as the difference between the total non-interference resistance and the interference of multihull ships, as stated by Sahoo *et al.,* [52] and Zhagi *et al.,* [53] . Interference effects can be expressed by the interference factor (IF) at Eq. (9). The interference factor contributed positively to reducing resistance, where the smaller the IF means the smaller the interference effect that occurs between the trimaran or pentamaran hulls and then produces minimum resistance. The IF graph for each trimaran and pentamaran model is shown in Figure 14.

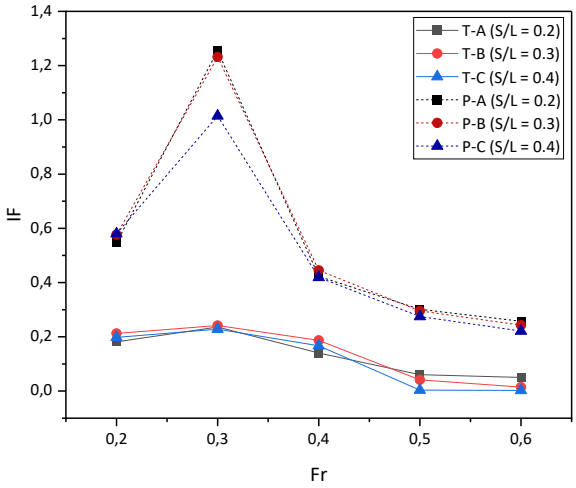

Fig. 14. Interference factor of trimaran and pentamaran

Figure 14 depicts T-C with Fr 0.6, showing the minimum IF because the separation distance is more significant than T-A and T-B. There are several aspects of the interference effect [54], namely; (a) Interaction of Kelvin waves generated by each ship hull, (b) changes in the wetted surface area (WSA) of individual hulls due to wave patterns generated by each hull and the pressure gradient that each hull creates over the other hull. Similar to the trimaran, the interference factor of the pentamaran decreases significantly at Fr > 0.3 and reaches its minimum at Fr 0.6. Additionally, P-C produces the smallest value at Fr > 0.2 than P-A and P-B. Hump and hollow phenomena may occur at a certain speed in a multihull vessel due to the interference of waves generated by each hull. Constructive wave interference produces a hump, adding to wave resistance, while destructive wave interference creates a hollow, potentially reducing wave resistance. Therefore, the optimal configuration for a multihull vessel is one with the lowest Interference Factor (IF) as explained by Souto-Iglesias *et al.,* [55].

The occurrence of wave breaking around the hull of the interference trimaran or pentamaran (bonded) makes this assumption too low in calculating the wave resistance component. Wave breaking is tough to measure directly, so it can only be visually observed, for example on the trimaran and pentamaran wave height contour in Figure 12 and Figure 13. Wave breaking occurs in the forward part of the hull (bow), and interference occurs in the midsection. Interference is affected by the S/L distance; the more significant the S/L distance, the less interference will occur, and conversely, the smaller the S/L distance, the more interference will occur; this only occurs at high speeds when Fr is 0.5 and 0.6.

4. Conclusion

In summary, this study extensively investigates the resistance characteristics of the trimaran and pentamaran configurations. This study utilized a comprehensive approach by integrating numerical and experimental analysis. The numerical method employs CFD simulation with Numeca software, using the unsteady RANS approach and the k-ω SST turbulence model. The CFD results were validated with the EFD results from the towing tank at ITS Surabaya. This dual methodology followed the ITTC formulas, standards, procedures, guidelines, and recommendations, thereby increasing the overall reliability of the study.

The results show that the trimaran consistently outperforms the pentamaran, exhibiting a smaller total resistance coefficient (C_T) with an average difference of 41.94%, particularly notable at Fr 0.3.

Configuration A, which features a low S/L ratio of 0.2 at a low Froude number (Fr), yields a smaller C_T than other configurations. An increase in friction resistance is observed up to a Froude number (Fr) of 0.4, followed by a decrease from 0.5 to 0.6. Notably, at Fr 0.2-0.3, friction resistance dominates the total resistance due to viscous factors, while at Fr 0.4, wave formation becomes the dominant factor contributing to the total resistance. The decline in total resistance at Fr 0.5 to 0.6 is attributed to wave interference causing cross-flow, especially away from the stern area of the trimaran.

The detailed component analysis shows that at Fr 0.2, wave resistance (C_W) for the trimaran accounts for only 12.13% of C_T, with friction resistance (C_F) dominating at 70.15%. C_W increases proportionally until Fr 0.4 but decreases to 29.99% at Fr > 0.4. In contrast, the pentamaran at Fr 0.2 has C_T at 16.75%, with C_F dominating at 62.95%. C_W increases to 44.24% at Fr 0.3-0.5 but decreases to 34.27% at Fr 0.6. The interference factor of the pentamaran decreases significantly at Fr > 0.3 and reaches its minimum at Fr 0.6. T-C with Fr 0.6, showing the minimum IF because the separation distance is more significant than T-A and T-B. Additionally, P-C produces the smallest value at Fr > 0.2 than P-A and P-B. The interference factor for wave resistance varies with S/L. As the separation distance between the hulls increases, the IF value becomes smaller. This is due to the height of the wave elevation being smaller, so there is a decrease in pressure between the hulls as the separation distance increases. Comparisons between Computational Fluid Dynamics (CFD) and Experimental Fluid Dynamics (EFD) results reveal that the trimaran consistently exhibits a smaller C_T than the pentamaran, with an average discrepancy of 15.06%. On average, discrepancies of 3.70% are observed between CFD and EFD results. The optimal configuration for a multihull vessel is one with the lowest Interference Factor (IF).

Acknowledgment
The first author thanks the Ministry of Education and Culture (Kemdikbudristek) for funding the study under a scheme called Postgraduate Education Scholarships within the Country (BPPDN) under contract numbers: T/56182/IT2/HK.00.01/2019 and 0626/E4/DT.04.02/2023.

References

[1] Gee, Nigel. "Future trends in high speed vessels." In *High Speed Vessels Future Development Conference, Victoria, Canada*. 1999.
[2] Peng, Hongxuan. "Numerical computation of multi-hull ship resistance and motion." (2001).
[3] Dubrovsky, Victor A. "Specificity and designing of multi-hull ships and boats." In *Specificity and Designing of Multi-Hull Ships and Boats*, pp. 1-217. 2016.
[4] Yuliora, E., I. K. A. P. Utama, and I. K. Suastika. "Numerical Study into the Resistance of a Trimaran Hull at Various Longitudinal Spacing." In *IOP Conference Series: Earth and Environmental Science*, vol. 1081, no. 1, p. 012056. IOP Publishing, 2022. https://doi.org/10.1088/1755-1315/1081/1/012056.
[5] Hafez, Khaled, and Abdel-Rahman El-Kot. "Comparative analysis of the separation variation influence on the hydrodynamic performance of a high speed trimaran." *Journal of Marine Science and Application* 10 (2011): 377-393. https://doi.org/10.1007/s11804-011-1083-0.
[6] Seif, Mohammad Saeed, and E. Amini. "Performance comparision between planing monohull and catamaran at high froude numbers." (2004): 435-441.
[7] Utama, I. K. A. P., and Ronald Mangasi Hutauruk. "A Study into the Selection of Mono-and Multi-Hull Vessel for Better Sea Transportation System." (2011).
[8] Nasirudin, Ahmad, I. Ketut Aria Pria Utama, and Andreas Kukuh Priyasambada. "CFD Analysis into the Resistance Estimation of Hard-Chine Monohull using Conventional against Inverted Bows." *CFD Letters* 15, no. 6 (2023): 54-64. https://doi.org/10.37934/cfdl.15.6.5464.

[9] Utama, I. K. A. P. "An Investigation into the Viscous Resistance Components of Catamarans." PhD diss., PhD Thesis, University of Southampton, UK, 1999.

[10] Suastika, Ketut, Ahmad Septiawan Saputra, Adnan Faiz Fauzi, and Ahmad Firdhaus. "Comparison of Performance of Straight-and V-shaped Vanes Applied as Energy Saving Device to High-speed Boats." *CFD Letters* 15, no. 10 (2023): 110-122. https://doi.org/10.37934/cfdl.15.10.110122.

[11] Yildiz, Burak, Bekir Sener, Suleyman Duman, and Raju Datla. "A numerical and experimental study on the outrigger positioning of a trimaran hull in terms of resistance." *Ocean Engineering* 198 (2020): 106938. https://doi.org/10.1016/j.oceaneng.2020.106938.

[12] Son, Changhwan, Prasanta K. Sahoo, Vaibhav Aribenchi, and Srikanth Asapana. "CFD Simulation of Resistance of Highspeed Trimaran Hullforms." In *SNAME International Conference on Fast Sea Transportation*, p. D011S001R006. SNAME, 2015. https://doi.org/10.5957/FAST-2015-011.

[13] Utama, I. K. A. P., and I. K. Suastika. "Experimental and Numerical Investigation into the Effect of the Axe-Bow on the Drag Reduction of a Trimaran Configuration." *International Journal of Technology* 12, no. 3 (2021): 527-538. https://doi.org/10.14716/ijtech.v12i3.4659.

[14] Dudson, Edward. "Optimisation of the seakeeping and performance of a 40-knot pentamaran container vessel." In *Proceedings of the 6th International Conference on Fast Sea Transportation FAST2001*, pp. 225-233. 2001.

[15] Yanuar, Ibadurrahman, R. Muhammad Arif, and D. P. Muhamad Ryan. "Resistance characteristic of high-speed unstaggered pentamaran model with variations of symmetric and asymmetric hull configurations." *Journal of Marine Science and Application* 18 (2019): 472-481. https://doi.org/10.1007/s11804-019-00119-0.

[16] Sulistyawati, Wiwin, M. Ammar Mahardika, and A. Azwin Alfarizsy. "Experimental hydrodynamic analysis of trimaran-pentamaran with variation transom non-transom on mainhull and sidehull." In *E3S Web of Conferences*, vol. 67, p. 04002. EDP Sciences, 2018. https://doi.org/10.1051/e3sconf/20186704002.

[17] Sulistyawati, Wiwin, Yanuar Yanuar, and Agus Sunjarianto Pamitran. "Research on pentamaran by model test and theoretical approach based on Michell's integral." *CFD Letters* 11, no. 3 (2019): 117-128.

[18] Andersson, Bengt, Ronnie Andersson, Love Håkansson, Mikael Mortensen, Rahman Sudiyo, and Berend Van Wachem. *Computational fluid dynamics for engineers*. Cambridge university press, 2011. https://doi.org/10.1017/CBO9781139093590.

[19] Nazemian, Amin, and Parviz Ghadimi. "Shape optimisation of trimaran ship hull using CFD-based simulation and adjoint solver." *Ships and Offshore Structures* 17, no. 2 (2022): 359-373. https://doi.org/10.1080/17445302.2020.1827807.

[20] Riyadi, Soegeng, and Ketut Suastika. "Experimental and Numerical Study of High Froude-number Resistance of Ship Utilizing a Hull Vane®: A Case Study of a Hard-chine Crew Boat." *CFD Letters* 12, no. 2 (2020): 95-105.

[21] Elhadad, Alaaeldeen M., and Abo El-Ela. "Experimental and Cfd Resistance Validation of Naval Combatant Dtmb 5415 Model." *Experimental and Cfd Resistance Validation of Naval Combatant Dtmb* 5415 (2023). https://doi.org/10.37934/arfmts.107.2.84102.

[22] Ibadurrahman, Ibadurrahman, A. Gunawan, and R. A. Wibowo. "Drag reduction of X-pentamaran ship model with asymmetric-hull outrigger configurations and hull separation." *Energy Reports* 6 (2020): 784-789. https://doi.org/10.1016/j.egyr.2019.11.158.

[23] Wang, S. M., W. Y. Duan, Q. L. Xu, F. Duan, G. Z. Deng, and Y. Li. "Study on fast interference wave resistance optimization method for trimaran outrigger layout." *Ocean Engineering* 232

(2021): 109104. https://doi.org/10.1016/j.oceaneng.2021.109104.

[24] Molland, A. "Resistance experiments on a systematic series of high speed catamaran forms: Variation of length-displacement ratio and breadth-draught ratio." *Trans Royal Inst Naval Archit* 138 (1996): 59-71.

[25] ITTC, Recommended Procedures. "Guidelines: Testing and Extrapolation Methods: Resistance-Uncertainty Analysis, Example for Resistance Test." *ITTC Recommended Procedures and Guidelines, Procedure* (2002): 7-5.

[26] Srinakaew, Sarawuth, D. J. Taunton, and D. A. Hudson. "Blockage effects on resistance prediction of high-speed catamarans." *Journal of Research and Applications in Mechanical Engineering* 7, no. 1 (2019): 23-32. https://doi.org/10.14456/jrame.2019.3.

[27] Fitriadhy, Ahmad, Nurul Shukna Rizat, Atiyah Raihanah Abd Razak, Sheikh Fakhruradzi Abdullah, Faisal Mahmuddin, and Alamsyah Kurniawan. "Optimization Modelling of a Catamaran Hull Form towards Reducing Ship's Total Resistance." *CFD Letters* 14, no. 4 (2022): 67-79. https://doi.org/10.37934/cfdl.14.4.6779.

[28] Waskito, Kurniawan Teguh. "On the High-Performance Hydrodynamics Design of a Trimaran Fishing Vessel." *Journal of Advanced Research in Fluid Mechanics and Thermal Sciences* 83, no. 1 (2021): 17-33. https://doi.org/10.37934/arfmts.83.1.1733.

[29] Royce, Richard, Jianjun Qi, Raju Datla, Jennifer Waters, Richard Bucknall, Alistair Greig, and Tristan Smith. "Facility comparison on model calm water resistance characteristics of a trimaran." In *SNAME American Towing Tank Conference*, p. D031S005R002. SNAME, 2010. https://doi.org/10.5957/ATTC-2010-026.

[30] Zhang, Bao-Ji, Sheng-Long Zhang, Bao-Ji Zhang, and Sheng-Long Zhang. "The optimization of the hull form with the minimum wave-making resistance based on potential flow theory." *Research on ship design and optimization based on simulation-based design (SBD) technique* (2019): 143-195. https://doi.org/10.1007/978-981-10-8423-2_5.

[31] Yanuar, Yanuar, Ibadurrahman Ibadurrahman, S. Karim, and M. Ichsan. "Experimental study of the interference resistance of pentamaran asymmetric side-hull configurations." In *AIP Conference Proceedings*, vol. 1826, no. 1. AIP Publishing, 2017. https://doi.org/10.1063/1.4979241.

[32] Molland, Anthony F., Stephen R. Turnock, and Dominic A. Hudson. *Ship resistance and propulsion*. Cambridge university press, 2017. https://doi.org/10.1017/9781316494196.

[33] Hafez, K. A., and A. A. El-Kot. "Comparative investigation of the stagger variation influence on the hydrodynamic interference of high speed trimaran." *Alexandria Engineering Journal* 51, no. 3 (2012): 153-169. https://doi.org/10.1016/j.aej.2012.02.002.

[34] Menter, Florianr. "Zonal two equation kw turbulence models for aerodynamic flows." In *23rd fluid dynamics, plasmadynamics, and lasers conference*, p. 2906. 1993.

[35] ITTC. (2011). "Fresh Water and Seawater Properties - 7.5-02-02-01.02," *26th Int. Towing Tank Conf. Rio Janeiro, Brazil, 28 August - 3 Sept.*, pp. 1–45.

[36] Allison, Chloe. "Meshing in FEA: Structured vs Unstructured meshes." *Blog, Onscale, April* 1 (2020).

[37] Deng, G. B., J. Piquet, X. Vasseur, and Michel Visonneau. "A new fully coupled method for computing turbulent flows." *Computers & Fluids* 30, no. 4 (2001): 445-472. https://doi.org/10.1016/S0045-7930(00)00025-6.

[38] Molland, A. F., and I. K. A. P. Utama. "Experimental and numerical investigations into the drag characteristics of a pair of ellipsoids in close proximity." *Proceedings of the Institution of Mechanical Engineers, Part M: Journal of Engineering for the Maritime Environment* 216, no. 2 (2002): 107-115. https://doi.org/10.1243/147509002762224324.

[39] Numeca International, "User Guide FINETM/Marine 9.2." in *Numeca Fine Open Manual Book*, Belgium, (2020).
[40] Zingg, D. "Viscous airfoil computations using Richardson extrapolation." In *10th Computational Fluid Dynamics Conference*, p. 1559. 1991. https://doi.org/10.2514/6.1991-1559.
[41] Celik, Ishmail B., Urmila Ghia, Patrick J. Roache, and Christopher J. Freitas. "Procedure for estimation and reporting of uncertainty due to discretization in CFD applications." *Journal of fluids Engineering-Transactions of the ASME* 130, no. 7 (2008). https://doi.org/10.1115/1.2960953.
[42] ITTC. (2021). "Uncertainty Recommended Analysis in CFD Verification and Validation Methodology and Procedures - 7.5-03-01-01."
[43] ITTC. (2021). "General Guideline for Uncertainty Analysis in Resistance Tests - 7.5-02-02-02."
[44] ITTC. (2021). "Example for Uncertainty Analysis of Resistance Tests in Towing Tanks - 7.5-02-02-02.1."
[45] Park, Dong-Min, Jaehoon Lee, and Yonghwan Kim. "Uncertainty analysis for added resistance experiment of KVLCC2 ship." *Ocean Engineering* 95 (2015): 143-156. https://doi.org/10.1016/j.oceaneng.2014.12.007.
[46] ISO, ISO. "98-3 guide to the expression of uncertainty in measurements, international organization for standardization: Geneva." (1995).
[47] Yanuar, Ibadurrahman, Kurniawan T. Waskito, S. Karim, and M. Ichsan. "Interference resistance of pentamaran ship model with asymmetric outrigger configurations." *Journal of Marine Science and Application* 16 (2017): 42-47. https://doi.org/10.1007/s11804-017-1401-2.
[48] Luhulima, Richard Benny, Sutiyo Sutiyo, and I. Utama. "The Resistance and EEDI Analysis of Trimaran Vessel with and without Axe-bow." *NAŠE MORE: znanstveni časopis za more i pomorstvo* 69, no. 3 (2022): 132-142.
[49] Hu, Pengwei, Ying Cui, Chenyu Zhao, Yanan Li, and Boyang Li. "Numerical Investigation on the Hydrodynamic Response of Pentamaran—Resistance Analysis of Different Outrigger Inclination Angles." *Journal of Marine Science and Engineering* 11, no. 1 (2023): 186. https://doi.org/10.3390/jmse11010186.
[50] Du, Lin, Hamid Hefazi, and Prasanta Sahoo. "Rapid resistance estimation method of non-Wigley trimarans." *Ships and Offshore Structures* 14, no. 8 (2019): 910-920. https://doi.org/10.1080/17445302.2019.1588499.
[51] Harvald S, Turnock S. R, and Hudson D. A. *"Resistance and Propulsion of Vessel."* Lyngby, Denmark: John Wiley & Sons., 1983.
[52] Sahoo, Prasanta K., Marcos Salas, and Adam Schwetz. "Practical evaluation of resistance of high-speed catamaran hull forms—Part I." *Ships and offshore structures* 2, no. 4 (2007): 307-324. https://doi.org/10.1080/17445300701594237.
[53] Zaghi, Stefano, Riccardo Broglia, and Andrea Di Mascio. "Analysis of the interference effects for high-speed catamarans by model tests and numerical simulations." *Ocean Engineering* 38, no. 17-18 (2011): 2110-2122. https://doi.org/10.1016/j.oceaneng.2011.09.037.
[54] Carr, Brendan, and R. Dvorak. "Investigation of trimaran interference effects." *Unpublished Bachelors Thesis, Webb Institute, Glen Cove, NY* (2007).
[55] Souto-Iglesias, Antonio, David Fernández-Gutiérrez, and Luis Pérez-Rojas. "Experimental assessment of interference resistance for a Series 60 catamaran in free and fixed trim-sinkage conditions." *Ocean Engineering* 53 (2012): 38-47. https://doi.org/10.1016/j.oceaneng.2012.06.008.